How to cite: *Angew. Chem. Int. Ed.* **2021**, *60*, 14480–14487
International Edition: doi.org/10.1002/anie.202101387
German Edition: doi.org/10.1002/ange.202101387

Dinitrogen Complexes

Merging Pincer Motifs and Potential Metal–Metal Cooperativity in Cobalt Dinitrogen Chemistry: Efficient Catalytic Silylation of N_2 to $N(SiMe_3)_3$

*Ming Li, Sandeep K. Gupta, Sebastian Dechert, Serhiy Demeshko, and Franc Meyer**

Dedicated to Prof. Gottfried Huttner

Abstract: *Using a pyrazolate-bridged dinucleating ligand that provides two proximate pincer-type PNN binding sites ("two-in-one pincer"), different synthetic routes have been developed towards its dicobalt(I) complex* ***2*** *that features a twice deprotonated ligand backbone and two weakly activated terminal N_2 substrate ligands directed into the bimetallic pocket. Protonation of* ***2*** *is shown to occur at the ligand scaffold and to trigger conversion to a tetracobalt(I) complex* ***4*** *with two end-on $\mu_{1,2}$-bridging N_2; in THF* ***4*** *is labile and undergoes temperature-dependent N_2/triflate ligand exchange. These pyrazolate-based systems combine the potential of exhibiting both metal–metal and metal–ligand cooperativity, viz. two concepts that have emerged as promising design motifs for molecular N_2 fixation catalysts. Complex* ***2*** *serves as an efficient (pre)catalyst for the reductive silylation of N_2 into $N(SiMe_3)_3$ (using KC_8 and Me_3SiCl), yielding up to 240 equiv $N(SiMe_3)_3$ per catalyst.*

Introduction

More than 99% of global nitrogen exists in the form of molecular N_2 in the atmosphere,[1] yet most organisms cannot metabolize the chemically inert N_2 but only nitrogenous substances such as ammonia (NH_3) or nitrate (NO_3^-).[2] Thus, the conversion of molecular N_2 into NH_3 or other useful chemical feedstocks is of fundamental importance.[3] In the biosphere, N_2 can be reduced under ambient conditions to ammonia by the FeMo-cofactor of nitrogenase via a sequence of electron and proton transfers,[4] while industrial nitrogen fixation is performed with H_2 at heterogenous Fe-based catalysts under high pressures and temperatures in the Haber–Bosch process.[5] Recent years have seen substantial research efforts devoted to the reductive cleavage and catalytic functionalization of N_2 under homogeneous conditions using molecular transition metal complexes.[6–12] While molybdenum catalysts are most prominent[13] and bioinspired approaches are focusing on iron complexes,[14,15] catalyst systems based on other earth abundant metals such as cobalt are also particularly attractive.

In that context an increasing number of cobalt dinitrogen complexes has been reported in recent years;[16] selected examples are depicted in Figure 1. Some of them have been

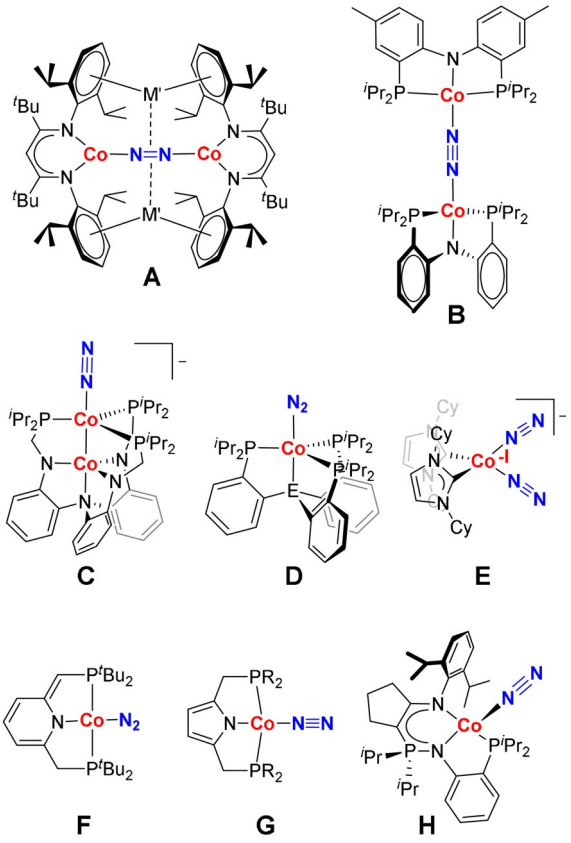

Figure 1. Selected examples of previously reported cobalt dinitrogen complexes (see text for references).

[*] Dr. M. Li, Dr. S. K. Gupta, Dr. S. Dechert, Dr. S. Demeshko, Prof. Dr. F. Meyer
Universität Göttingen, Institut für Anorganische Chemie
Tammannstrasse 4, 37077 Göttingen (Germany)
E-mail: franc.meyer@chemie.uni-goettingen.de
Homepage: http://www.meyer.chemie.uni-goettingen.de
Prof. Dr. F. Meyer
Universität Göttingen, International Center for Advanced Studies of Energy Conversion (ICASEC)
Tammannstrasse 6, 37077 Göttingen (Germany),
and
Universität Göttingen, Wöhler Research Institute for Sustainable Chemistry (WISCh)
Tammannstrasse 2, 37077 Göttingen (Germany)
Supporting information and the ORCID identification number(s) for the author(s) of this article can be found under: https://doi.org/10.1002/anie.202101387.

shown to mediate the catalytic formation of NH_3 from N_2 using KC_8 and a proton source, with low turnover numbers (TONs). For example, complex **D**[17] (E = B; using 60 equiv of KC_8) gave 2.4 equiv[17a] and complex **G**[18] (with 200 equiv KC_8) gave 17.9 equiv of NH_3.

Catalytic silylation of N_2 with an excess of $SiMe_3Cl$ under reductive conditions, first reported by Shiina for simple metal halide salts using Li wire as a reducing agent,[19] is an interesting alternative for N_2 valorization; the formed silylamines can also be hydrolyzed to NH_3. This reaction is generally assumed to proceed via the in situ generation of silyl radicals, and complexes of a variety of metal ions have been shown to catalyze N_2 silylation.[20] In a systematic study evaluating the effect of 3d metal ion type on N_2 silylation by polynuclear complexes of Cr, Mn, Fe, Co and Ni, Murray et al. recently demonstrated the superiority of Co for this reaction ($\approx$200 equiv $N(SiMe_3)_3$/Co_3-complex).[21] In most reported cases, however, TONs (i.e., equiv of $N(SiMe_3)_3$ formed per equiv of catalyst) are still <100.[12,20] The Nishibayashi group developed an efficient catalytic system, *trans*-$[Mo(N_2)_2(depf)_2]$ (depf = 1,1′-bis(diethylphosphino)ferrocene) which mediated the conversion of N_2 to $N(SiMe_3)_3$ with a TON of 226 when using 8000 equiv of Na and $SiMe_3Cl$.[22] In the case of Co, the best performing systems so far are the anionic dicobalt complex **C** based on a trisphosphino(triamido)amine scaffold developed by Lu et al. (using 2000 equiv KC_8 and $SiMe_3Cl$)[23] and the iminophosphorane-cobalt derivative **H** reported by Fryzuk, Masuda et al. (1500 equiv KC_8 and 2000 equiv $SiMe_3Cl$);[24] both systems catalyze the conversion of N_2 to $N(SiMe_3)_3$ with TONs of $\approx$200. Deng et al. showed that reactions of NHC-ligated low-valent Co complexes such as $[(ICy)_2Co(N_2)_2]^-$ (**E**; TON $\approx$120 for N_2 silylation with 2000 equiv KC_8 and $SiMe_3Cl$) with SiR_3Cl (R = Me, Et) result in the formation of diazene complexes $[(ICy)_2Co(\eta^2\text{-}R_3SiNNSiR_3)]$, suggesting that they represent intermediates in the catalytic cycle.[25]

Two conceptual approaches have emerged as promising design guidelines for N_2 fixation with molecular catalysts, both in Co/N_2 chemistry and beyond: (i) the use of tridentate pincer-type ligand scaffolds[26] (see, e.g., **B**,[27] **F**,[28] **G**[18] and **H**[24] in Figure 1)[29] that potentially allow for metal–ligand cooperativity (MLC)[30] and (ii) the use of bimetallic systems that synergistically achieve the overall 6 e^- reduction required to fully cleave N_2 (e.g., **A**,[31] **B**[27,32] and **C**[23] in Figure 1) and that potentially exploit metal–metal cooperativity (MMC). In order to combine these two features in a single platform, we recently developed a so-called "two-in-one pincer" ligand that provides two PNN pincer-type binding sites fused via a central pyrazolate (Figure 2).[33] A diiron complex $LFe_2(OTf)_3(CH_3CN)$ of the compartmental ligand $[L]^-$ was shown to undergo rapid ligand exchange reactions (coupled to spin transitions)[33] within the bimetallic pocket into which the two accessible coordination sites X of the pincer subunits are directed, and we demonstrated that double backbone dearomatization in dirhodium(I) complexes of $[L]^-$ is possible via sequential deprotonation at the side-arm methylene groups.[34] We have now exploited the "two-in-one pincer" platform in Co/N_2 chemistry, and we show that some of the new dinuclear cobalt complexes serve as efficient precatalysts for the silylation of N_2 into $N(SiMe_3)_3$, producing up to $\approx$240 equiv $N(SiMe_3)_3$.

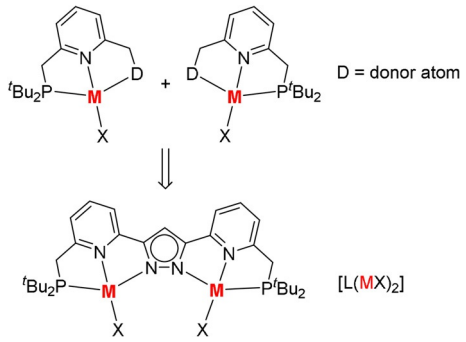

Figure 2. Conceptual merging of two pincer-type subunits in the pyrazolate-based "two-in-one" pincer platform $[L]^-$.

Results and Discussion

As an entry into cobalt coordination chemistry of the pyrazolate-based "two-in-one" pincer ligand $[L]^-$, the proligand HL was treated with one equivalent of KO^{t}Bu and two equivalents of $CoCl_2$ in THF to generate a blue suspension from which, after workup, the dicobalt(II) complex $[L(CoCl)_2(\mu\text{-}Cl)]$ (**1**) was isolated (Scheme 1). Blue rod-shaped crystals were obtained by slow diffusion of pentane into a CH_2Cl_2 solution of **1**, with an excellent yield of 90%. The molecular structure of complex **1** (Figure 3) determined by X-ray diffraction confirms that the two cobalt ions are hosted in the tridentate {PNN} binding sites of the anionic compartmental ligand scaffold, bridged by the pyrazolate and an exogenous chloride. Each metal ion has an additional terminal chlorido ligand which completes an overall distorted square-pyramidal coordination environment ($\tau_5 = 0.31$ and 0.27).[35] The comparatively long Co–Cl2 (2.44/2.46 Å) and Co1–N3/Co2–N4 bonds (2.24/2.26 Å; compared to Co1–N1/Co2–N2 which are 2.00/2.01 Å) indicate that the relatively wide Co···Co separation imposed by the binucleating scaffold (3.81 Å in **1**) leads to some strain and significant deviation of the N3/4-Co-Cl2 angles from linearity (N3-Co1-Cl2: 158.7°, N4-Co2-Cl2: 152.8°).

Positive-ion electrospray ionization mass spectrometry (ESI(+)-MS; Figure S5) of a solution of **1** in MeCN shows a dominant peak at $m/z = 725.1$ corresponding to the cation $[LCo_2Cl_2]^+$, evidencing that the dinuclear core remains intact in solution. The ^{1}H NMR spectrum of complex **1** in $CDCl_3$ (Figure S1) exhibits eight resonances between −11 and 86 ppm at room temperature, in accordance with paramagnetism and C_2 symmetry. No signals were observed in the ^{31}P NMR spectrum, presumably because of the vicinity of the nuclei to paramagnetic metal ions. Variable-temperature magnetic susceptibility data recorded with a SQUID magnetometer confirm the presence of two high-spin cobalt(II) ions ($S = 3/2$) that are antiferromagnetically coupled to give an $S = 0$ ground state; the best fit of the data leads to $g = 2.4$ and an exchange coupling $J = -7.2$ cm^{-1} (Figure S7).

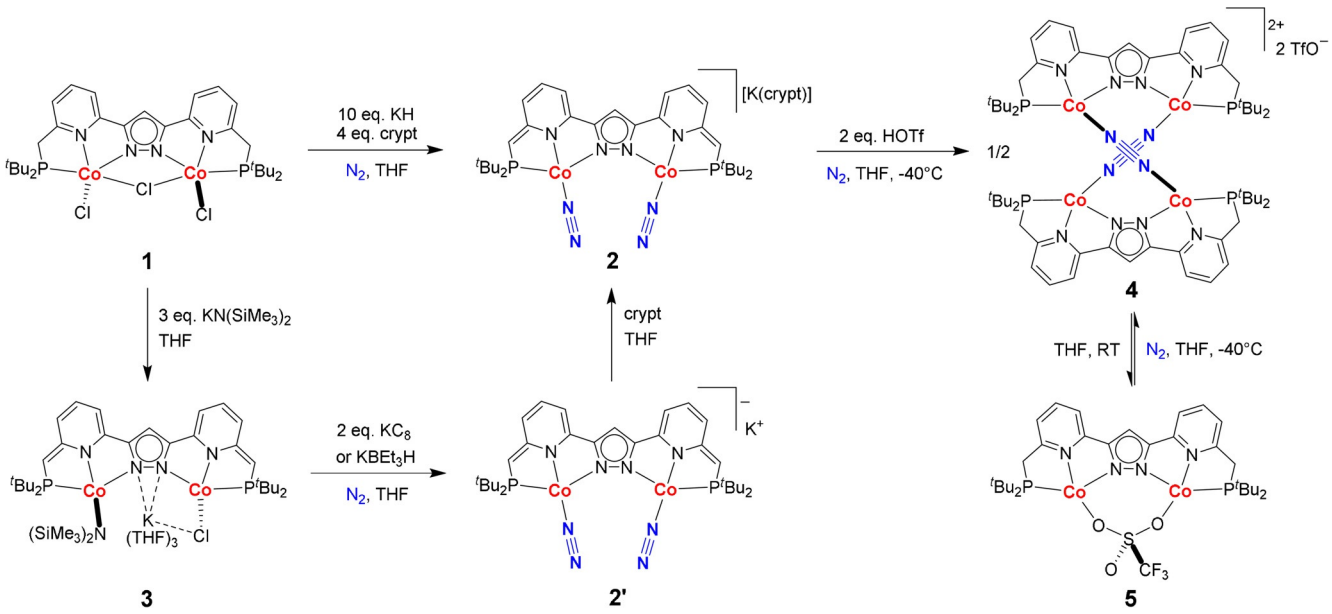

Scheme 1. New compounds and their synthetic transformations reported in this work.

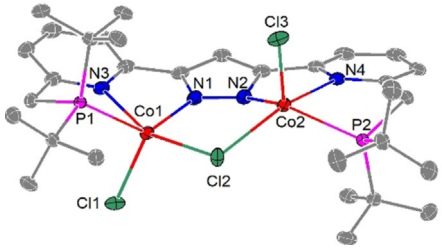

Figure 3. Molecular structure of **1** (30% probability thermal ellipsoids); hydrogen atoms omitted for clarity.

In literature reports, $Co(N_2)$ complexes are often obtained from the reaction of a suitable cobalt halide precursor with strong reductants such as Na/Hg, $Na(C_{10}H_8)$ or KC_8 under N_2 atmosphere.[16] In the present case, however, treatment of complex **1** with an excess of the above reductants proved unsuccessful but led to unidentified products. In contrast, addition of ten equivalents of KH and four equivalents of [2.2.2]cryptand to a solution of complex **1** in THF under N_2 atmosphere in a one-pot reaction gave rise to a dark blue solution, from which the highly air-sensitive complex $[L'-(CoN_2)_2][K([2.2.2]cryptand)]$ (**2**) could be isolated in 55% yield ($[L']^{3-}$ is the twice deprotonated derivative of $[L]^-$); complex **2** shows characteristic UV-Vis absorptions at $\lambda_{max} =$ 335, 479, 521 and 621 nm (Figure S17). The molecular structure of the anion of **2** determined by X-ray diffraction is shown in Figure 4; the potassium cation is encapsulated by the [2.2.2]cryptand and is thus separated from the anion. Selected bond lengths and angles are listed in Table 1.

The two cobalt ions in **2** are found in roughly square-planar coordination environment, nested in the {PNN} compartments of the dinucleating ligand scaffold and spanned by the pyrazolato bridge. The planarity of the peripheral chelate rings and inspection of bond lengths reveals that the two methylene groups of the "two-in-one" pincer are deprotonated in **2**, which is accompanied by dearomatization of the pyridine rings, giving a trianionic ligand $[L']^{3-}$.[34] Most

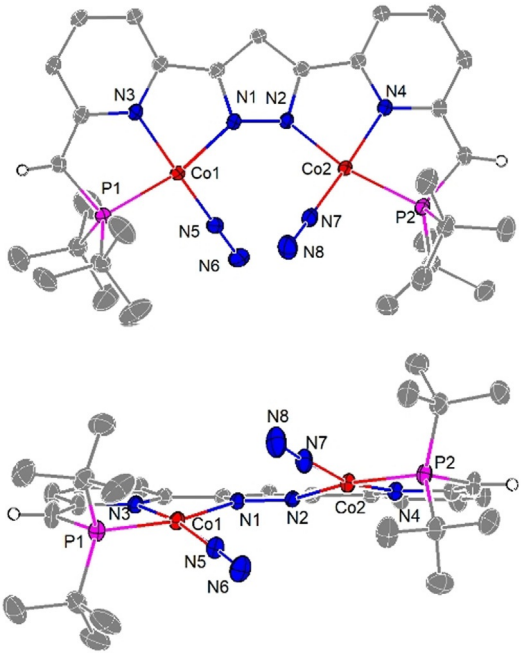

Figure 4. Top view (top) and front view (bottom) of the molecular structure of the anion of **2** (30% probability thermal ellipsoids); most hydrogen atoms omitted for clarity.

Table 1: Selected interatomic distances [Å] and angles [°] of **2** and **4**.

	2	4
Co···Co [Å]	4.30	4.35, 4.41, 4.44, 4.68, 4.69
N–N [Å]	1.124(3)/ 1.125(3)	1.140(5)/ 1.142(6)
Co–N(N_2) [Å]	1.742(2)/ 1.742(2)	1.764(4) –1.783(4)
Co-N-N(N_2) [°]	173.8(2)/ 174.7(2)	174.4(4) –176.9(4)

indicative is the shortening of the exocyclic C–C bonds in the side arms from 1.506(3)/1.507(3) Å in complex **1** to 1.372(3)/1.384(3) Å in complex **2**. The coordination sphere of each cobalt ion in **2** is completed by an end-on bound N_2 that is oriented into the bimetallic pocket. The N≡N bond lengths of the coordinated N_2 molecules are 1.124(3) and 1.125(3) Å, which is consistent with those in previously reported $Co^I(N_2)$ complexes such as **D**[17c] (E = Si, 1.123(3) Å), **F**[28] (1.122(2) Å), and **H**[24] (1.12(6) Å) in Figure 1 and not much longer than in free N_2 (1.098 Å);[36] this corroborates that **2** is best described as having two Co^I (d^8, $S=0$) ions and weakly activated N_2. The Co···Co separation in **2** of 4.30 Å is distinctly longer by 0.49 Å than in complex **1**, and the Co-N-N-Co torsion angle is quite large (34.2°). This reflects the congestion caused by the two N_2 ligands coming into steric clash within the bimetallic pocket, forcing them to point below or above the equatorial plane defined by the pyrazolate heterocycle. The results in (non-crystallographic) C_2 symmetry of the anion of **2**, with both enantiomers present in the crystal.

The ^{1}H NMR spectrum of **2** in [D_8]THF shows that complex **2** is a diamagnetic species, in accordance with the presence of two Co^I (d^8, $S=0$) ions (Figure S8). Apparent C_{2v} symmetry in solution indicates that interconversion of the two enantiomeric forms is rapid on the NMR time scale, even at 203 K (Figure S11). The ^{31}P NMR spectrum reveals a peak at 81.3 ppm (Figure S12), and the ^{15}N NMR spectrum of the isotopically labeled complex **2**-$^{15}N_2$ shows two resonances at $\delta = -28.6$ and -58.1 ppm (Figure S16); the latter signal at higher field is assigned to N_α of the coordinated dinitrogen molecules, the former signal to N_β (N_α is the atom bound to the metal and N_β is the terminal atom). Complex **2**-$^{15}N_2$ can be readily prepared from **2** via ligand exchange under $^{15}N_2$ atmosphere at room temperature, indicating that the N_2 ligands are rather labile.

The IR spectrum of solid **2** show two intense N_2 isotope sensitive bands at 2032 and 2009 cm^{-1} that shift to 1973 and 1950 cm^{-1} upon $^{15}N_2$ labelling ($\Delta(^{15}N_2–^{14}N_2) = -59\ cm^{-1}$, $\tilde{\nu}(^{14}N–^{14}N)/\tilde{\nu}(^{15}N–^{15}N) = 1.030$, calculated 1.035 for an isolated harmonic N–N oscillator) (Figure 5). Based on the DFT calculated IR spectrum (Figure S82) the two bands are assigned to the antisymmetric and symmetric N–N stretches, respectively, indicating substantial vibrational coupling. The frequencies for **2** are similar to those of other pincer ligated Co^I complexes with end-on bound N_2 (cf. 2021 cm^{-1} for **F**, ≈2020 cm^{-1} for **G**, 2071 cm^{-1} for **H**; Figure 1) and reflect weak activation of the N_2 ligand (N-N stretch of free N_2 at 2331 cm^{-1}).[37]

In the absence of cryptand, the reaction of complex **1** with excess KH in THF generates a brown solution that contains both diamagnetic and paramagnetic species according to NMR spectroscopy; however, these species could not be identified. The cryptand obviously plays a crucial role in the reaction of KH with complex **1** to give complex **2**, likely via improving the solubility and/or increasing the reactivity of KH in THF. Since KH serves both as a base and a reductant in this transformation, a stepwise synthetic route was developed (Scheme 1). To that end, complex **1** was first reacted with three equivalents of the base $KN(SiMe_3)_2$ in THF at room temperature, leading to an immediate color change of the solution to red. The new dicobalt(II) complex [L′(CoN($SiMe_3$)$_2$)(CoCl)(K(THF)$_3$)] (**3**) (Figure 6) could be isolated, and crystals suitable for X-ray diffraction were grown by layering a concentrated THF solution with hexanes at −40 °C. **3** features the twice deprotonated ligand $[L']^{3-}$ with dearomatized pyridines (the exocyclic C–C bonds in the side arms are 1.366(3) and 1.381(3) Å), a large Co···Co separation of 4.54 Å (0.24 Å longer than in **2**) and a wide Co-N-N-Co torsion angle of 62.0°. One equivalent of the formed KCl is still retained in the structure of **3**. The ^{1}H NMR spectrum of **3** in [D_8]THF displays paramagnetically shifted resonances (Figure S18). Magnetic susceptibility data (SQUID) indeed revealed weakly antiferromagnetically coupled $S=3/2$ and $S=1/2$ cobalt(II) ions ($J=-1.0\ cm^{-1}$); the former is tentatively assigned to the distorted tetrahedral Co1 ($\tau_4=0.71$)[38] and the latter to the roughly square-planar Co2 ($\tau_4=0.21$) (Figure S20).

Subsequent reduction of dicobalt(II) complex **3** was achieved by either $KHBEt_3$ or KC_8 (2 equiv) in THF solution under N_2 atmosphere. The resulting complex **2′** could be isolated by precipitation from a mixture of THF and hexanes

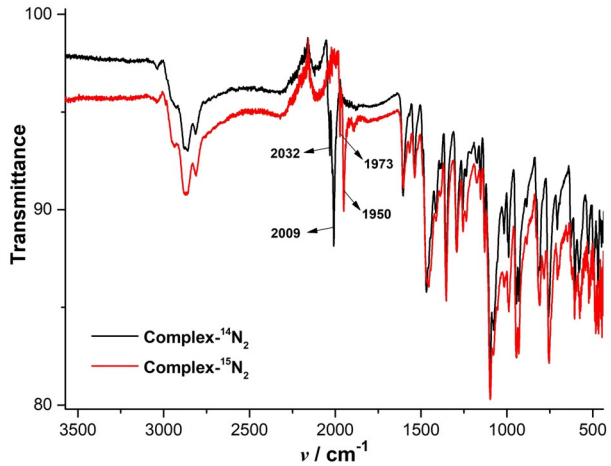

Figure 5. IR spectra of solid **2** prepared under $^{14}N_2$ (black spectrum) and $^{15}N_2$ (red spectrum).

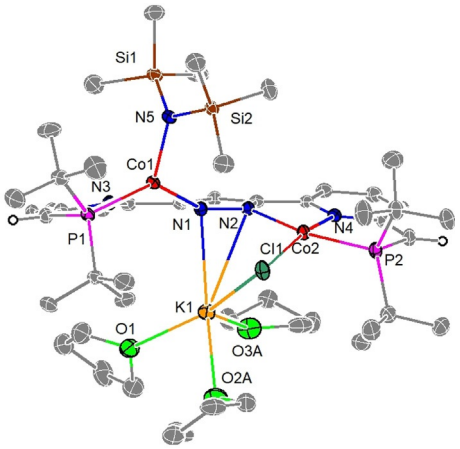

Figure 6. Molecular structure of **3** (30% probability thermal ellipsoids); most hydrogen atoms omitted for clarity.

at −40 °C; however, crystallization was unsuccessful so far. The IR spectrum of **2′** shows N–N stretching vibrations at 2044 and 2004 cm^{-1} that shift to 1979 and 1953 cm^{-1} upon $^{15}N_2$ labelling (Figure S30). The ^{1}H NMR spectrum of complex **2′** in [D_8]THF (Figure S21) is very similar to the spectrum of **2** (except for the missing cryptand signals and the presence of non-deuterated THF that likely serves as a ligand to K^+ in the isolated material of **2′**); it shows that **2′** is a diamagnetic complex that exhibits apparent C_{2v} symmetry on the NMR time scale. Also the ^{31}P NMR spectrum ($\delta = 81.4$ ppm; Figure S25) as well as the ^{15}N NMR spectrum of **2′**-$^{15}N_2$ ($\delta = -28.9$ and −57.9 ppm, assigned to N_β and N_α of coordinated N_2 molecules, respectively; Figure S29) are very similar to the ones of **2**. Addition of one equivalent of [2.2.2]cryptand to **2′** readily gives complex **2** in 90 % yield. The combined findings confirm that **2′** is a $[K(THF)_x]^+$ salt of $[L'(CoN_2)_2]^-$; the slight shift in IR bands for the N–N stretches compared to **2** suggests some interaction of K^+ with the anion, but details remain unclear as long as crystallographic insight is lacking. This multistep route via **3** and **2′** provides an alternative and more favorable synthesis of complex **2**.

As N_2 reduction is commonly assumed to proceed through coupled H^+/e^- transfer pathways, protonation of complexes **2** and **2′** was studied individually. Treatment of complexes **2** or **2′** in THF with two equivalents of triflic acid (HOTf) under N_2 atmosphere at −40 °C resulted in an immediate color change of the solution from dark blue to red-brown. Block-shaped crystals suitable for X-ray diffraction analysis were grown from the concentrated red-brown THF solution at −40 °C and revealed the formation of a tetracobalt complex with two bridging N_2 ligands $[(LCo_2)_2(\mu\text{-}N_2)_2)](OTf)_2$ (**4**; Figure 7). Complex **4** features two {LCo_2} subunits, and metric parameters of the aromatic pyridine rings as well as the lengths of the exocyclic C–C bonds (1.490(8)–1.511(7) Å) confirm that protonation has occurred at the ligand side arms. The cobalt ions are found in distorted square-planar environment with Co···Co distances of 4.35/4.44 Å within the {LCo_2} subunits (Table 1). The protonated ligand scaffold appears to be quite flexible as the {LCo_2} strands are twisted to minimize deviation from the square-planar metal coordination sphere, leading to large Co-N-N-Co torsion angles of 68.2° and 70.0°. The two {LCo_2} fragments in **4** are linked by two end-on bridging N_2 ligands with N–N bond lengths (1.140(5)/1.142-(6) Å) that are slightly longer than in **2** because of charge transfer to the N_2-ligand from two metal ions, but in the range typical for previously reported Co^I-($\mu_{1,2}$-N_2)-Co^I systems.[27,31] The Co–N_α(N_2) bonds in **4** (1.764(4)–1.783(4) Å) are slightly longer than in **2** (1.742(2) Å), reflecting diminished π-back-donation for the individual Co→N_2 interactions and likely weakened Co–N_2 bonding; the latter is evidenced in solution by facile temperature-dependent replacement of the N_2 ligands by triflate (see below).

The N-N stretching vibrations of **4** could not be observed by IR spectroscopy (Figure S45), but a Raman spectrum of solid **4** shows a weak absorption at 2000 cm^{-1} that shifts to 1935 cm^{-1} for **4**-$^{15}N_2$ ($\Delta(^{15}N_2$–$^{14}N_2) = -65$ cm^{-1}, $\tilde{\nu}$ (^{14}N–^{14}N)/$\tilde{\nu}$(^{15}N–^{15}N) = 1.034, calculated 1.035 for an isolated harmonic N-N oscillator; Figure 8). Comparison of the N–N bond lengths and the N–N stretching frequencies indicates that the bridging N_2 in complex **4** is more reduced than the end-on bound N_2 in complex **2**, but still rather weakly activated (cf. 2024 cm^{-1} in **B**).

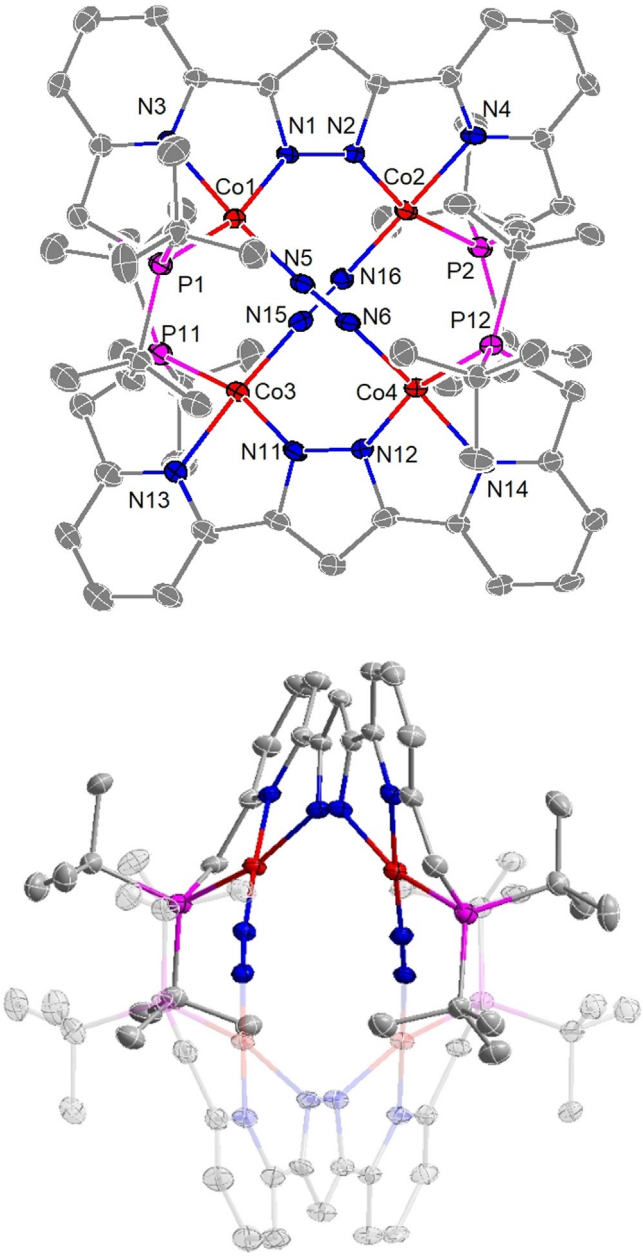

Figure 7. Two different views of the molecular structure of the cation of **4** (30 % probability thermal ellipsoids); hydrogen atoms omitted for clarity.

The UV-Vis spectrum of solid **4** shows a broad band at ≈ 670 nm and further bands at 517 and 323 nm (Figure S47). However, variable temperature (VT) UV-Vis spectra of **4** in THF in the range from 298 K to 233 K indicate some complex solution equilibria (Figure 9). The UV-Vis spectrum of **4** in THF at 298 K shows that the band at 670 nm is absent, but the spectrum indicates the presence of a new species **5** with λ_{max} at 313, 510 and 774 nm. After cooling the THF solution to 233 K under Ar the spectrum remains essentially unchanged (Figure S58). Under N_2 at 233 K, however, the spectrum gradually changes as the band at 774 nm disappears over the course of

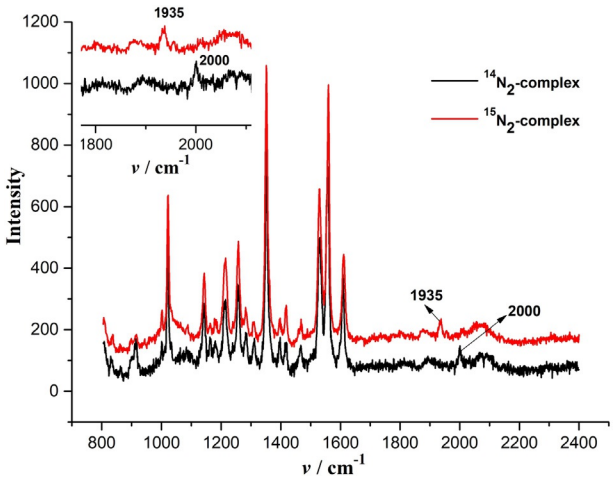

Figure 8. Raman spectra of solid samples of **4** (black) and **4**-$^{15}N_2$ (red); inset showing the spectra in the range of 1800–2100 cm^{-1}.

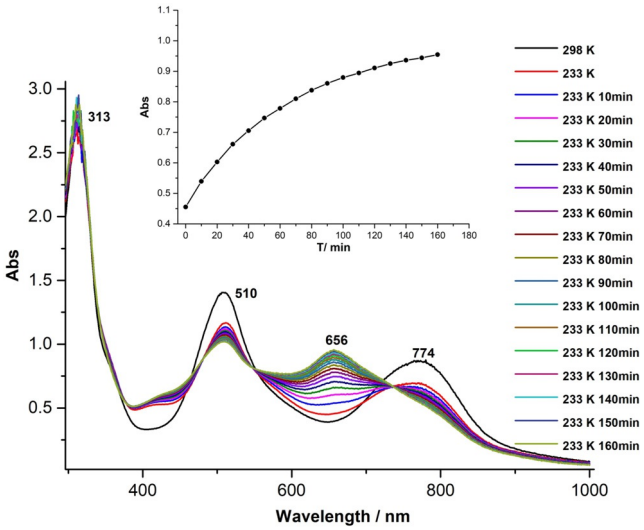

Figure 9. UV-Vis spectra of complex **4** in THF solution under N_2 atmosphere at 298 K and 233 K, and time dependence of the spectra at 233 K; inset showing increasing intensity of the band at 656 nm and the formation of **4** at 233 K.

several hours while a prominent absorption at 656 nm emerges, with isosbestic points at 481, 547, and 736 nm. The process is reversible upon warming and suggests binding of N_2 to form **4** at lower temperatures; the characteristic electronic absorption at 656 nm is assigned to a Co→N_2 MLCT transition in **4**, which is absent in **5**.

Slow diffusion of pentane into the THF solution of complex **4** at room temperature yielded block-shaped crystals of the neutral complex [LCo_2(μ-OTf)] (**5**); X-ray diffraction shows the two metal ions in square planar geometry, bridged by a μ-η^1:η^1 triflate anion hosted within the bimetallic pocket (Figure 10). SQUID magnetometry reveals that solid **5** is diamagnetic throughout the entire temperature range, in accordance with Co^I (d^8, $S=0$) ions (Figure S60). When a THF solution of complex **5** under N_2 was cooled to −40 °C, crystals of the tetracobalt(I) complex **4** formed, confirming

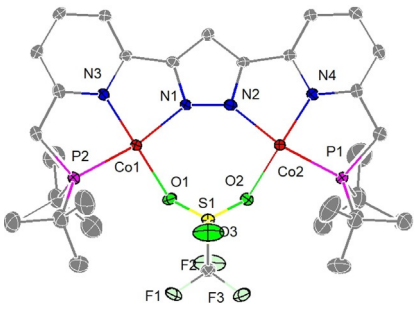

Figure 10. Molecular structure of **5** (30% probability thermal ellipsoids); hydrogen atoms omitted for clarity.

the reversibility of N_2 binding in solution and the conclusions drawn from VT UV-Vis spectroscopy.

Temperature-dependent equilibria involving **4** and **5** in solution are also evidenced by VT NMR spectroscopy (Figure S32 and S48). Complex **5** at 238 K under Ar exhibits the spectral pattern expected for a C_{2v} symmetric complex (six resonances in the ^{1}H NMR spectrum, Figure S49; $\delta(^{31}P)=$ 219.0 ppm, Figure S56) and the ^{19}F-NMR spectrum at 213 K shows a single peak at −77.7 ppm for bound triflate (Figure S57). Upon warming the signals shift and broaden, suggesting paramagnetic contributions at higher temperatures possibly caused by fast equilibria arising from triflate/THF ligand exchange. Under N_2 atmosphere the VT NMR spectra of **4** and **5** are identical, and at high temperatures they are essentially identical to the ones of **5** recorded under Ar atmosphere. In [D_8]THF under N_2 at 238 K and below, the signal pattern reflects the reduced symmetry of diamagnetic **4** with two resonances each for the diastereotopic *t*Bu groups and for the protons of the CH_2 groups in Figure S33 (and $\delta(^{31}P)_{238K}=99.5$ ppm in Figure S40). The sharp ^{19}F NMR signal at −78.8 ppm for **4** at 213 K broadens and shifts to −75.5 ppm at 298 K (Figure S43). ^{1}H DOSY spectra (using the solvent signal as an internal standard)[39] recorded in [D_8]THF at 238 K for **4** under N_2 and for **5** under Ar confirm their different nuclearity (Figure S34, S44 and S50): the tetracobalt complex **4** has a diffusion coefficient $D=1.293\times10^{-10}$ m^2s^{-1} corresponding to a hydrodynamic radius $r=$ 13.81 Å (derived from the Stokes–Einstein equation),[40] while dicobalt complex **5** has $D=2.507\times10^{-10}$ m^2s^{-1} ($r=$ 7.12 Å) which is similar to the values for the free ligand HL at 238 K ($D=2.306\times10^{-10}$ m^2s^{-1}, $r=7.74$ Å).[41]

Having established the identity of the Co/N_2 complexes of the two-in-one pincer scaffold in the solid state and in solution, their ability to mediate the catalytic silylation of N_2 in the presence of an excess of KC_8 (2000 equiv) and $SiMe_3Cl$ (2000 equiv) in THF has been studied (Table 2). The product $N(SiMe_3)_3$ was identified by GC/MS and quantified by GC using cyclododecane as the internal standard. Complex **2** is a very efficient catalyst that generates $N(SiMe_3)_3$ in 22.4% yield (150 equiv $N(SiMe_3)_3$ per catalyst or 75 equiv $N(SiMe_3)_3$ per Co atom) at room temperature. The yield rises to 36.0% (240 equiv $N(SiMe_3)_3$/catalyst) when the reaction is first conducted at −40 °C for 2 h before warming to room temperature; when carried out at −90 °C for 2 h the yield is 32.9% (219 equiv $N(SiMe_3)_3$/catalyst; see entries 4–6 in Table 2). These values compare favorably with the most active

Table 2: Reductive silylation of N_2 to $N(SiMe_3)_3$ using complexes **1**, **2**, **2′**, **3** and **5** as catalysts.

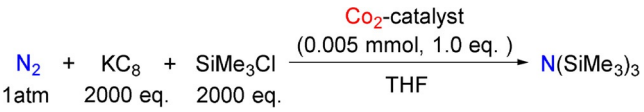

Entry	Catalyst	Conditions	$N(SiMe_3)_3$ (mmol)[a]	$N(SiMe_3)_3$/catalyst[b] ($N(SiMe_3)_3$/Co atom)	Yield [%][c]
1	**5**	−40 °C 2 h; r.t. 22 h	1.04	208 (104)	31.2
2	**2′**	−40 °C 2 h; r.t. 22 h	1.17	234 (117)[e]	35.1
3	**3**	−40 °C 2 h; r.t. 22 h	1.14	228 (114)	34.2
4	**2**	−40 °C 2 h; r.t. 22 h	1.20	240 (120)	36.0
5	**2**	−90 °C 2 h; r.t. 22 h	1.10	219 (109.5)	32.9
6	**2**	r.t. 24 h	0.75	150 (75)	22.4
7	**1**	−40 °C 2 h; r.t. 22 h	0.95	190 (95)	28.5
8	2.0 equiv. $CoCl_2$	−40 °C 2 h; r.t. 22 h	0.58	58 (58)[d]	17.4
9	2.0 equiv. $CoCl_2$	r.t. 24 h	0.1	10 (10)[d]	3.0
10	none	−40 °C 2 h; r.t. 22 h	0	0 (0)	0

[a] $N(SiMe_3)_3$ was identified by GC/MS and quantified by GC with cyclododecane as the internal standard. All values are the average of at least three trials. [b] Calculated as the molar ratio of $N(SiMe_3)_3$ to catalyst. [c] The yields of $N(SiMe_3)_3$ are based on starting material $SiMe_3Cl$. [d] per Co. [e] Acid hydrolysis of $N(SiMe_3)_3$ and quantification of the formed NH_4^+ by ^1H NMR spectroscopy using an internal standard (average of three trials, see Supporting Information for details) yielded 230 equiv NH_4^+/catalyst (115 equiv NH_4^+/Co atom).

molecular catalysts for N_2 silylation reported to date (compare Table S4).[12,20] When using the same conditions (−40 °C for 2 h, then room temperature; see Table 2) also dicobalt complexes **1** (190 equiv $N(SiMe_3)_3$/catalyst), **2′** (234 equiv $N(SiMe_3)_3$/catalyst), **3** (228 equiv $N(SiMe_3)_3$/catalyst) and **5** (208 equiv $N(SiMe_3)_3$/catalyst) serve as efficient catalysts. Complex **2** appears to be the most active, but given that all these systems based on the $\{LCo_2\}$ or $\{L'Co_2\}$ scaffold give roughly comparable yields of $N(SiMe_3)_3$ (in the range 190–240 equiv) it is well conceivable that they form the same catalytic species when applying identical reaction protocols. In independent experiments using **2′** as a selected catalyst under typical reaction conditions, the formed $N(SiMe_3)_3$ was converted to ammonia via acid hydrolysis and the resulting NH_4^+ quantified by ^1H NMR spectroscopy, confirming comparable yields of $N(SiMe_3)_3$ and NH_4^+ (234 equiv vs. 230 equiv per catalyst, respectively; see entry 2 and footnote in Table 2).

Other products generated in the challenging silylation reaction were identified and quantified by GC/MS (see Supporting Information for details). These include hexamethyldisilane, *n*-butoxytrimethylsilane and trimethyl(4-(trimethylsilyl)butoxy)silane, the latter two resulting from ring cleavage and silylation of THF by $Me_3Si^\bullet$ radicals under the harsh reaction conditions, as reported previously.[42] Silyl ether formation, specifically the formation of significant amounts of trimethyl(4-(trimethylsilyl)butoxy)silane (see Table S3), consumes substantial reducing equivalents and $SiMe_3Cl$, which may contribute to limiting the yield of $N(SiMe_3)_3$ to below 40 % based on the reagent $SiMe_3Cl$ (see Table 2). Future work will target potential mechanisms of the N_2 silylation reaction, specifically the possible involvement of MLC or MMC, and the isolation of intermediates.

Conclusion

This work commences the exploration of dinuclear complexes of the pyrazolate-based "two-in-one pincer" ligand, which features two pyridyl-centered PNN compartments, in dinitrogen fixation chemistry. Such systems bear the potential of combining in a single platform two cooperativity concepts that have emerged as promising approaches for molecular N_2 fixation catalysis, viz., functional tridentate pincer sites that may undergo reversible ligand-centered (de)protonation associated with pyridyl (de)aromatization, and bimetallic scaffolds that provide a multi-electron reservoir for challenging substrate reductions. Cobalt(I) dinitrogen complexes of the bis(PNN) pincer ligand have been isolated, and it is demonstrated that protonation at the ligand backbone leads to release of terminal N_2 to give a labile tetracobalt(I) complex with two central Co-($\mu_{1,2}$-N_2)-Co entities. Using $SiMe_3Cl$ in the presence of the reducing agent KC_8, the new dinuclear cobalt complexes have been shown to mediate the silylation of N_2 to $N(SiMe_3)_3$ producing up to 240 equiv $N(SiMe_3)_3$ per catalyst (or 120 equiv $N(SiMe_3)_3$ per Co atom), which are among the highest reported so far for this reaction. Future work will focus on mechanistic insight and on the possible role of metal–ligand and metal–metal cooperativity for this and related N_2 transformations catalyzed by the highly preorganized "two-in-one pincer" based bimetallic complexes.

Experimental Section

General experimental details and characterization data for all of the reported compounds are included in the Supporting Information. Deposition Numbers 2054109, 2054110, 2054111, 2054112, and 2054113 contain the supplementary crystallographic data for this paper. These data are provided free of charge by the joint Cambridge Crystallographic Data Centre and Fachinformationszentrum Karlsruhe Access Structures service www.ccdc.cam.ac.uk/structures.

Acknowledgements

Support from the China Scholarship Council (Ph.D. fellowship for M.L.) and the University of Göttingen (F.M.) is gratefully acknowledged. S.K.G. thanks the Alexander von Humboldt Foundation for a postdoctoral research fellowship. This project has been partly funded by the Deutsche Forschungsgemeinschaft (DFG, German Research Foundation)—project number INST 186/1329-1 FUGG (SQUID

magnetometer). Open access funding enabled and organized by Projekt DEAL.

Conflict of interest

The authors declare no conflict of interest.

Keywords: cobalt · dinitrogen complexes · dinuclear complexes · nitrogen fixation · pincer ligands

[1] a) P. Warneck, J. Williams, *The Atmospheric Chemist's Companion: Numerical Data for Use in the Atmospheric Sciences*, Dordrecht, Springer, **2012**; b) N. Gruber, J. N. Galloway, *Nature* **2008**, *451*, 293 – 296.

[2] a) Q. Cheng, *J. Integr. Plant Biol.* **2008**, *50*, 786 – 798; b) D. E. Canfield, A. N. Glazer, P. G. Falkowski, *Science* **2010**, *330*, 192 – 196; c) B. Thamdrup, *Annu. Rev. Ecol. Evol. Syst.* **2012**, *43*, 407 – 428.

[3] J. G. Chen, R. M. Crooks, L. C. Seefeldt, K. L. Bren, R. M. Bullock, M. Y. Darensbourg, P. L. Holland, B. Hoffman, M. J. Janik, A. K. Jones, M. G. Kanatzidis, P. King, K. M. Lancaster, S. V. Lymar, P. Pfromm, W. F. Schneider, R. R. Schrock, *Science* **2018**, *360*, eaar6611.

[4] a) B. M. Hoffman, D. Lukoyanov, Z. Yang, D. R. Dean, L. C. Seefeldt, *Chem. Rev.* **2014**, *114*, 4041 – 4062; b) O. Einsle, D. C. Rees, *Chem. Rev.* **2020**, *120*, 4969 – 5004.

[5] R. Schlögl, *Angew. Chem. Int. Ed.* **2003**, *42*, 2004 – 2008; *Angew. Chem.* **2003**, *115*, 2050 – 2055.

[6] Y. Nishibayashi in *Transition Metal-Dinitrogen Complexes: Preparation and Reactivity* (Ed.: Y. Nishibayashi), Wiley-VCH, Weinheim, **2019**, pp. 1 – 77.

[7] M. D. Fryzuk, S. A. Johnson, *Coord. Chem. Rev.* **2000**, *200 – 202*, 379 – 409.

[8] a) Y. Nishibayashi, *Inorg. Chem.* **2015**, *54*, 9234 – 9247; b) Y. Nishibayashi, *Dalton Trans.* **2018**, *47*, 11290 – 11297.

[9] Y. Tanabe, Y. Nishibayashi, *Chem. Rec.* **2016**, *16*, 1549 – 1577.

[10] N. Stucke, B. M. Flöser, T. Weyrich, F. Tuczek, *Eur. J. Inorg. Chem.* **2018**, 1337 – 1355.

[11] "Nitrogen Fixation": I. Klopsch, E. Y. Yuzik-Klimova, S. Schneider in *Topics in Organometallic Chemistry*, *Vol. 60* (Ed.: Y. Nishibayashi), Springer, Heidelberg, **2017**, pp. 71 – 112.

[12] F. Masero, M. A. Perrin, S. Dey, V. Mougel, *Chem. Eur. J.* **2021**, *27*, 3892 – 3928.

[13] "Nitrogen Fixation": A. Eizawa, Y. Nishibayashi in *Topics in Organometallic Chemistry*, *Vol. 60* (Ed.: Y. Nishibayashi), Springer, Heidelberg, **2017**, pp. 1 – 21.

[14] I. Djurdjevic, O. Einsle, L. Decamps, *Chem. Asian J.* **2017**, *12*, 1447 – 1455.

[15] a) "Nitrogen Fixation": A. L. Speelman, P. L. Holland in *Topics in Organometallic Chemistry*, *Vol. 60* (Ed.: Y. Nishibayashi), Springer, Heidelberg, **2017**, pp. 197 – 213; b) A. D. Piascik, A. E. Ashley in *Transition Metal-Dinitrogen Complexes: Preparation and Reactivity* (Ed.: Y. Nishibayashi), Wiley-VCH, Weinheim, **2019**, pp. 285 – 335.

[16] C. C. Lu, S. D. Prinslow in *Transition Metal-Dinitrogen Complexes: Preparation and Reactivity* (Ed.: Y. Nishibayashi), Wiley-VCH, Weinheim **2019**, pp. 337 – 402.

[17] a) T. J. Del Castillo, N. B. Thompson, D. L. M. Suess, G. Ung, J. C. Peters, *Inorg. Chem.* **2015**, *54*, 9256 – 9262; b) D. L. M. Suess, C. Tsay, J. C. Peters, *J. Am. Chem. Soc.* **2012**, *134*, 14158 – 14164; c) M. T. Whited, N. P. Mankad, Y. Lee, P. F. Oblad, J. C. Peters, *Inorg. Chem.* **2009**, *48*, 2507 – 2517.

[18] S. Kuriyama, K. Arashiba, H. Tanaka, Y. Matsuo, K. Nakajima, K. Yoshizawa, Y. Nishibayashi, *Angew. Chem. Int. Ed.* **2016**, *55*, 14291 – 14295; *Angew. Chem.* **2016**, *128*, 14503 – 14507.

[19] K. Shiina, *J. Am. Chem. Soc.* **1972**, *94*, 9266 – 9267.

[20] Y. Tanabe, Y. Nishibayashi, *Coord. Chem. Rev.* **2019**, *389*, 73 – 93.

[21] M. C. Eaton, B. J. Knight, V. J. Catalano, L. J. Murray, *Eur. J. Inorg. Chem.* **2020**, 1519 – 1524.

[22] H. Tanaka, A. Sasada, T. Kouno, M. Yuki, Y. Miyake, H. Nakanishi, Y. Nishibayashi, K. Yoshizawa, *J. Am. Chem. Soc.* **2011**, *133*, 3498 – 3506.

[23] R. B. Siedschlag, V. Bernales, K. D. Vogiatzis, N. Planas, L. J. Clouston, E. Bill, L. Gagliardi, C. C. Lu, *J. Am. Chem. Soc.* **2015**, *137*, 4638 – 4641.

[24] T. Suzuki, K. Fujimoto, Y. Takemoto, Y. Wasada-Tsutsui, T. Ozawa, T. Inomata, M. D. Fryzuk, H. Masuda, *ACS Catal.* **2018**, *8*, 3011 – 3015.

[25] Y. Gao, G. Li, L. Deng, *J. Am. Chem. Soc.* **2018**, *140*, 2239 – 2250.

[26] a) H. Tanaka, Y. Nishibayashi, K. Yoshizawa, *Acc. Chem. Res.* **2016**, *49*, 987 – 995; b) I. Klopsch, M. Finger, C. Wuertele, B. Milde, D. B. Werz, S. Schneider, *J. Am. Chem. Soc.* **2014**, *136*, 6881 – 6883; c) R. S. van Alten, F. Waetjen, S. Demeshko, A. J. M. Miller, C. Wuertele, I. Siewert, S. Schneider, *Eur. J. Inorg. Chem.* **2020**, 1402 – 1410.

[27] A. R. Fout, F. Basuli, H. Fan, J. Tomaszewski, J. C. Huffman, M. Baik, D. J. Mindiola, *Angew. Chem. Int. Ed.* **2006**, *45*, 3291 – 3295; *Angew. Chem.* **2006**, *118*, 3369 – 3373.

[28] S. P. Semproni, C. Milsmann, P. J. Chirik, *J. Am. Chem. Soc.* **2014**, *136*, 9211 – 9224.

[29] Further examples of Co/N_2 complexes based on pincer-type ligands: a) J. Scott, S. Gambarotta, I. Korobkov, *Can. J. Chem.* **2005**, *83*, 279 – 285; b) A. C. Bowman, C. Milsmann, C. C. H. Atienza, E. Lobkovsky, K. Wieghardt, P. J. Chrik, *J. Am. Chem. Soc.* **2010**, *132*, 1676 – 1684; c) S. Rozenel, R. Padilla, J. Arnold, *Inorg. Chem.* **2013**, *52*, 11544 – 11550; d) C. A. Sanz, C. A. M. Stein, M. D. Fryzuk, *Eur. J. Inorg. Chem.* **2020**, 1465 – 1471.

[30] a) C. Gunanathan, D. Milstein, *Acc. Chem. Res.* **2011**, *44*, 588 – 602; b) D. Milstein, *Philos. Trans. R. Soc. London Ser. A* **2015**, *373*, 1 – 10.

[31] K. Ding, A. W. Pierpont, W. W. Brennessel, G. Lukat-Rodgers, K. R. Rodgers, T. R. Cundari, E. Bill, P. L. Holland, *J. Am. Chem. Soc.* **2009**, *131*, 9471 – 9472.

[32] For a complex closely related to **B** see: J. Choi, Y. Lee, *Angew. Chem. Int. Ed.* **2019**, *58*, 6938 – 6942; *Angew. Chem.* **2019**, *131*, 7012 – 7016.

[33] S. Samanta, S. Demesko, S. Dechert, F. Meyer, *Angew. Chem. Int. Ed.* **2015**, *54*, 583 – 587; *Angew. Chem.* **2015**, *127*, 593 – 597.

[34] A. Gers-Barlag, P. Goursot, M. Li, S. Dechert, F. Meyer, *Eur. J. Inorg. Chem.* **2019**, 3329 – 3334.

[35] A. W. Addison, T. N. Rao, J. Reedijk, J. Van Rijn, G. C. Verschoor, *J. Chem. Soc. Dalton Trans.* **1984**, 1349 – 1356.

[36] R. J. Le Roy, Y. Huang, C. Jary, *J. Chem. Phys.* **2006**, *125*, 164310.

[37] B. P. Stoicheff, *Can. J. Phys.* **1954**, *32*, 630 – 634.

[38] L. Yang, E. R. Powell, R. P. Houser, *Dalton Trans.* **2007**, 955 – 964.

[39] D. J. Metz, A. Glines, *J. Phys. Chem.* **1967**, *71*, 1158.

[40] A. Einstein, *Ann. Phys.* **1905**, *322*, 132.

[41] Quantitative comparison is not possible because of the non-spherical shape and different charges of the compounds.

[42] a) M. Yuki, H. Tanaka, K. Sasaki, Y. Miyake, K. Yoshizawa, Y. Nishibayashi, *Nat. Commun.* **2012**, *3*, 1254; b) K. Ishihara, Y. Araki, M. Tada, T. Takayama, Y. Sakai, W. M. C. Sameera, Y. Ohki, *Chem. Eur. J.* **2020**, *26*, 9537 – 9546.

Manuscript received: January 28, 2021
Accepted manuscript online: April 8, 2021
Version of record online: May 19, 2021

